MethodsX 17 (2026) 104132

Contents lists available at ScienceDirect

MethodsX

journal homepage: www.elsevier.com/locate/methodsx

Using Landsat, Sentinel-1 and -2 and GEE to assess changes in wetland Ecosystem Functional Groups in the Maputaland Coastal Plain of South Africa

Philani Apleni [a], Laven Naidoo [a,b], Philemon Tsele [a], Heidi van Deventer [a,c,*]

[a] Department of Geography, Geoinformatics & Meteorology, University of Pretoria, Private Bag X20, Hatfield, Pretoria, 0028, South Africa
[b] Gauteng City-Region Observatory (GCRO), a Partnership of the University of Johannesburg, the University of the Witwatersrand, Johannesburg, the Gauteng Provincial Government and Organised Local Government in Gauteng (SALGA), Johannesburg, South Africa
[c] Council for Scientific and Industrial Research (CSIR), PO Box 395, Pretoria, 0001, South Africa

GRAPHICAL ABSTRACT

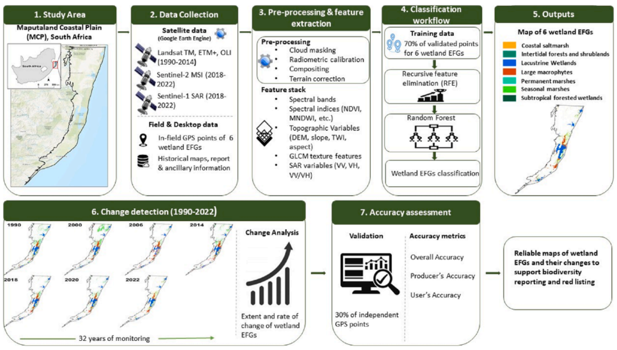

ARTICLE INFO

Dataset link: https://doi.org/10.71506/csirza.32006340

Keywords:
Earth Observation
Global Biodiversity Framework (GBF)
Google Earth Engine (GEE)

ABSTRACT

Consistent monitoring of wetland Ecosystem Functional Groups (EFGs) over large areas and long periods remains challenging owing to uneven availability, varying spatial resolutions, and spectral similarity of some EFGs. A Google Earth Engine (GEE)-based Earth Observation workflow was developed to map and quantify changes in wetland EFGs across the Maputaland Coastal Plain (MCP) in South Africa. The study included Landsat imagery for 1990, 2000, 2006 and 2014; and Sentinel-1 and Sentinel-2 imagery for 2018, 2020 and 2022. The methods involved:

* Corresponding author.
E-mail address: HvDeventer@csir.co.za (H. van Deventer).

https://doi.org/10.1016/j.mex.2026.104132
Received 11 May 2026; Accepted 28 August 2026
Available online 29 August 2026

Random Forest
Remote Sensing

- Data collection of historical desktop datasets and in-field validation of seven wetland EFG types;
- Multiple spectral indices derived from the images were combined with topographical variables and elevation data derived from a Digital Terrain Model, as well as desktop and in-field-collected data points in a classification algorithm;
- Recursive feature elimination was used to select the most informative predictors; and
- The use of a Random Forest machine learning algorithm and recursive feature elimination for the classifications in GEE.

Changes in EFGs were quantified between 1990 and 2022. The classification algorithm can be used recursively, while only the input point datasets should be iteratively validated using fine-scale spatial-resolution data, such as aerial or orthophotos, or in-field validation. The methods improved the delineation of the seven wetland EFGs compared to other datasets and contributed to the Red List of Ecosystems (RLE) assessment of the EFGs.

Specifications table.

Subject area	Earth and Planetary Sciences
More specific subject area	Using Earth Observation methods to determine changes in wetland Ecosystem Functional Groups towards Red Listing of Ecosystems
Name of your method	Classification approach in mapping wetland Ecosystem Functional Groups and determining these changes over time
Name and reference of original method	[1]. A land use and land cover classification system for use with remote sensor data (Vol. 964). US Government Printing Office.
Resource availability	Google Earth Engine (https://earthengine.google.com/)

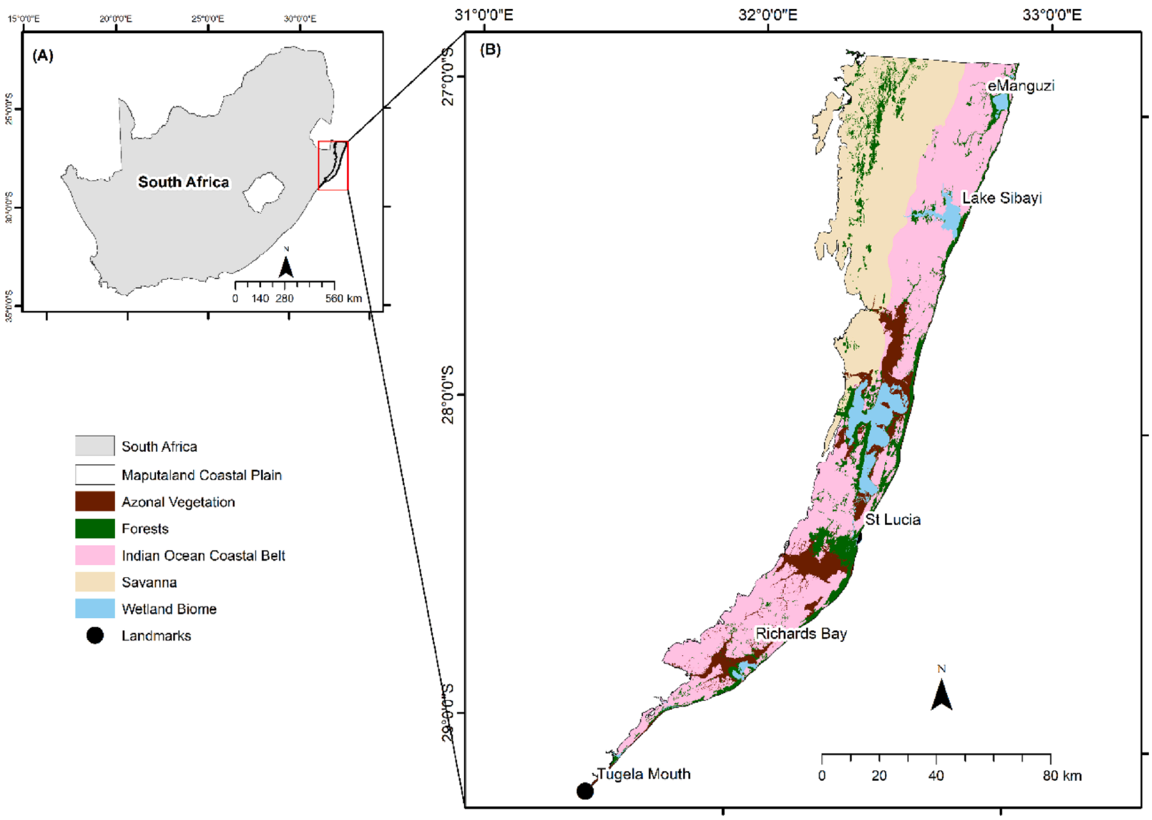

Fig. 1. Location of the Maputaland Coastal Plain (MCP) relative to (a) South Africa, providing (b) an overview of the MCP showing the extent of wetlands mapped in the National Wetland Map version 5 [5], some key vegetation biomes [6] and main landmarks and towns.

Background

Cloud computing capabilities developed for Earth Observation (EO) images offer a practical means of tracking the extent and rate of change in the globe's most threatened ecosystem type: wetlands. Wetland EFGs are linked wetland ecosystems within the wetland biome with shared ecological causes and dependencies, resulting in convergent biotic features [2]. These groups simplify complex wetland ecosystems based on similar vegetation species or communities, allowing for analysis of disturbance responses, resilience to invasions, and prediction of community shifts due to human-induced changes or climate change. Combining EO imagery, particularly from the freely available Landsat and Sentinel missions that cover 60 years and more, with machine-learning classification methods enables multi-decadal tracking of the extent and rate of change that EFGs undergo under shifting climatic and human-driven pressures. This paper describes a detailed workflow that uses the Random Forest classification algorithm to classify the extent and rate of change in seven EFGs at a regional scale for the MCP over 32 years, drawing on archival optical and Synthetic Aperture Radar (SAR) data. The data were analysed in Google Earth Engine (GEE; [3]) and incorporated spectral indices, topographic variables, and variable-importance selection. The resulting 2022 map was validated against an extensive set of field-collected Global Positioning System (GPS) points of the six palustrine wetland EFGs collected across the study area, whereas the seventh EFG, lacustrine wetlands, was modelled at a desktop level. This approach produced more accurate outcomes than comparable extents mapped in other local and global wetland ecosystem type classification products. Given the workflow's robustness, which draws on cloud computing, machine learning, an extensive EO archive, and carefully curated input parameters within GEE, the methodology is transferable to other wetland regions worldwide where floristic types can be distinguished and used for biodiversity reporting and Red Listing of Ecosystems (RLE).

Method details

The methods below are presented in several subsections: first, the study area description; then, the analytical framework, data collection procedures, and satellite image pre-processing; the classification and finally, the accuracy evaluation.

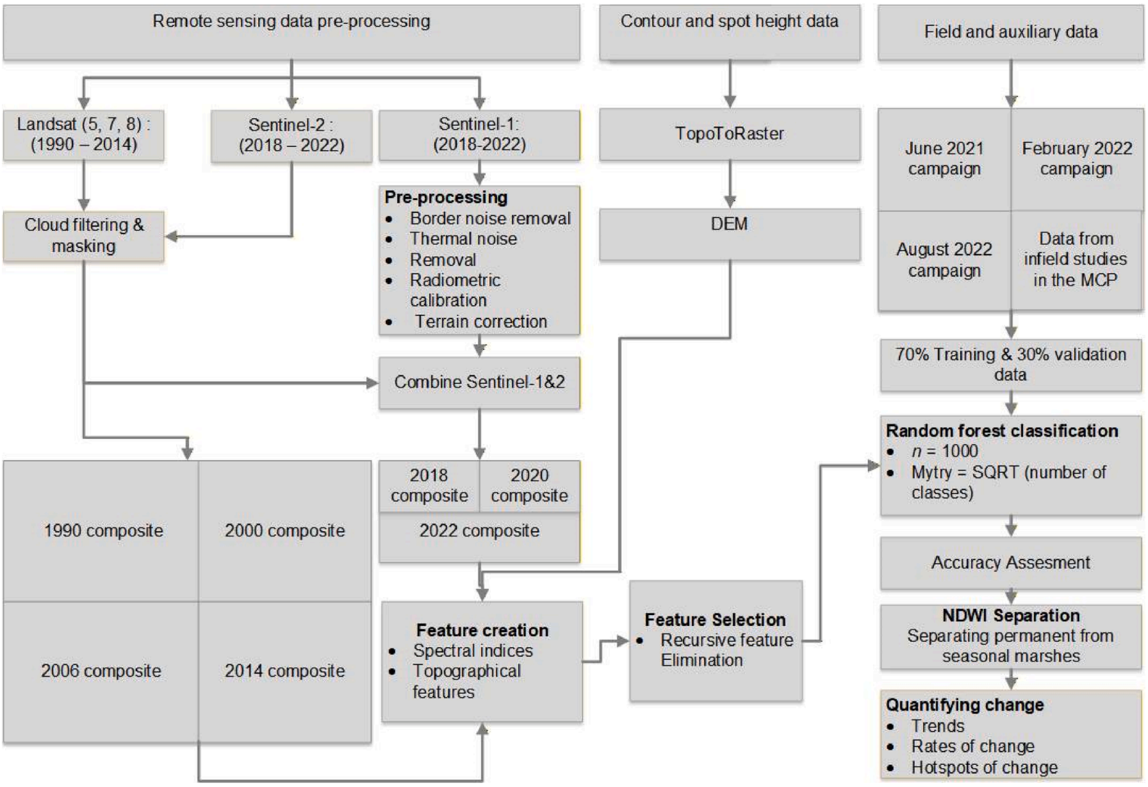

Fig. 2. Overview of the workflow of the wetland Ecosystem Functional Groups classification in GEE, which includes pre-processed image inputs, the consideration of supplementary datasets to refine the classification, the application of field validation points, and the image classification and accuracy-assessment methods used in this study. DEM = digital elevation model; MCP = Maputaland Coastal Plain; NDWI = normalised difference water index; SQRT = square root.

Description of the study area

The MCP is located in South Africa, on the north-eastern coastal region south of Mozambique (Fig. 1). It covers a total of 8 141 km^2 within the range of latitude between 29°13′22.913″ S and 26°50′56.266″ S and longitude between 31°30′19.69″ E and 32°53′27.806″ E in the KwaZulu-Natal Province (see [4] for the full description of the study area and map).

Methodological framework

The approach and workflow (Fig. 2) outline the methodology applied to the detection and quantification of changes in the locations, rates, and extents of wetland EFG across the MCP. The workflow begins by gathering reference samples to train a Random Forest classification algorithm for each yearly median composite. Rainfall records were examined, with particular attention to wet years, to help capture the maximum extent of wetlands. Classifications for 1990 to 2014 relied on Landsat imagery, while the 2018–2022 analyses drew on Sentinel-1 and −2 imagery. Spectral, topographical and textural features, together with elevation data, were then merged with these images to improve classification performance. A feature-selection step was applied to isolate the most useful predictors for classifying wetland types, and an accuracy assessment verified the reliability of the resulting classifications. Finally, the methodology calculates the rate of change in wetland EFGs and pinpoints hotspots of substantial change, alongside projections of likely future states. Further detail on each of these steps follows in the sections below.

Step 1: Collect reference and in-field validation data for wetland EFGs

Reference sample points representing the wetland EFGs within the MCP were gathered in two stages. The initial stage entailed assembling all existing mapped and published wetland and terrestrial-class information for the MCP (Table 1). Selected areas and points from these datasets were considered (Table 2), and used to build regions of interest (ROIs) for classification (Table 3), which was especially useful for historical years lacking field data.

All points were first reprojected into the South African Albers Equal Area (AEA) coordinate system, using 25°E as the central meridian and standard parallels at 24°S and 33°S [35]. The second stage centred on field validation, with emphasis placed on areas that earlier studies had covered less thoroughly. Wetland classes followed the Global Ecosystem Typology (GET) at the EFG level [33], with 'Large macrophytes' appended as an additional class based on earlier EO work demonstrating that this group could be reliably delineated [34]. In this study area, Large macrophytes comprise wetland vegetation typically taller than 4 m, including bulrush (*Typha capensis*), common reed (*Phragmites australis*), Lowveld reed (*Phr. mauritianus*), paper reed (*Cyperus papyrus*), and saw-grass (*Cladium mariscus*). Ground data supporting the wetland EFG classification were gathered across three separate field campaigns. The first, held from 6 to 11 June 2021, concentrated largely on the northern MCP; the second, from 6 to 11 February 2022, targeted the southern MCP; and the third, from 15 to 19 August 2022, aimed to validate preliminary classifications and focused on the far northern MCP (Fig. 3). Point locations of the EFGs were captured from homogeneous patches of at least 30 × 30 m using a handheld Garmin 62-s GPS unit, with a spatial accuracy of 4 m. Each point was logged as a waypoint number and recorded in a datasheet, along with a description of the dominant EFG present. Across the three campaigns, 551 points were collected in total (Table 3); 371 of these (67%) fell within the extent of protected areas mapped in the South African National Protected Areas Database [36], and the remaining 180 (33%) lay outside these. These points fed directly into the 2022 classification, while additional terrestrial classes were sourced from other studies, as listed in Table 3.

For 1990, 2000, 2006, 2014, 2018, 2020 and 2022, the field data and information drawn from previous studies formed the primary

Table 1
Summary of studies that mapped wetland biomes or ecosystem functional group classes using remote sensing and satellite imagery on the Maputaland Coastal Plain (MCP), showing the extent of wetlands mapped, the wetland types identified, and whether changes in wetland extent were quantified over time.

Study	Area mapped (km^2), with the percentage of the extent relative to the MCP in brackets (%)	Wetland types classified	Change detection of wetland extent and type
Bessinger et al. [7]	3 871 km (5.7)	Lacustrine wetlands, intertidal forests and shrublands, and Herbaceous coastal wetlands	No
Dlamini et al. [8]	~134 (1.6)	Lacustrine and grouped palustrine wetlands	Yes, between 1997 and 2017
Grundling et al. [9]	~943 (11.6)	Lacustrine, Wetlands (Sedge/moist grassland), Swamp forests	Yes, 1992 and 2008
Lück-Vogel et al. [10]	305 (3.7)	Mangroves, Open water, Reed-sedge, Swamp forests	No
Ramjeawon et al. [11]	2 587 (31.8)	Lacustrine and grouped palustrine wetlands	Yes, between 1986 and 2019
Slagter et al. [12]	1 400 (17)	High-vegetated, Low-vegetated, Medium-vegetated	No
Van Deventer et al. [13]	1 753 (21.5)	Six forested wetland species	No
Van Deventer et al. [14]	1 753 (21.5)	Large macrophytes, Mangrove ferns, Mangrove forests, Seasonal wetlands	No

Table 2
Inventory of data used in the Earth Observation (EO) classification of wetland Ecosystem Functional Groups (EFGs) in the Maputaland Coastal Plain (MCP). GTI = Geo Terra Image; ROIs = Regions of interest.

Title of study	Description of the data used	How the data was prepared for use in the EO classification	Source
Vegetation classification and description of five wetland systems and their respective zones on the MCP.	Point and polygon dataset of floristic sample points (relevés) with vegetation descriptions that include large macrophytes, seasonal and permanent marshes and swamp forests in the Muzi swamp system.	Used to inform points for marsh wetlands, large macrophytes and subtropical-temperate forested wetlands.	Pretorius [15]
Analysis of three decades of land cover changes in the MCP, South Africa.	Raster dataset of predicted extent of the timber plantations in northern MCP.	Used to inform points for the selection of timber plantations.	Ramjaewon et al. [11]
Assessing subtropical forest fragmentation for DukuDuku forest.	A point dataset containing sample sites of terrestrial forest species, with some related to freshwater ecosystems.	Some points were selected for classifying terrestrial forests (coastal forests). A few points of *Bridelia micrantha* could not be revisited during fieldwork to validate their extent relative to the Landsat and Sentinel-2 pixels.	Cho et al. [16,17]
Conservation conundrum – Red listing of subtropical-temperate coastal forested wetlands of South Africa.	Polygon data with digitised terrestrial and forested wetland extents covering the whole MCP.	Used to select ROIs of subtropical-temperate forested wetlands and terrestrial forests.	Van Deventer et al. [18]
Distribution and long-term historic impact of small-scale subsistence farming on wetlands in the MCP, KwaZulu-Natal, South Africa.	A dataset containing the locations of historically degraded wetlands in the MCP (relic gardens).	Used to select cultivated wetland and relic garden points.	Arndt [19]
Forest and woodland expansion into forestry plantations informs screening for native agroforestry species, MCP, South Africa.	Dataset with points with descriptions of terrestrial forests/ woodland and timber plantations.	Used to select ROI points for timber plantations and terrestrial forests.	Starke et al. [20]
National Peatlands Database.	Ground sampled points of locations of peatlands around South Africa.	Data were corrected and some points were used to inform areas of forested wetlands, marshes and large macrophytes wetland EFGs.	Grundling et al. [21]
National Wetland Vegetation Database (NWVD).	A point data set containing a floristic sampling of vegetation clusters at wetland points in South Africa.	Points identified with high confidence were used directly in the classification, while other points informed the ROIs.	Sieben et al. [22]
Satellite-imagery-based classification of near-natural and used wetlands in a subtropical region. A case study on the impact of subsistence farming on the MCP, South Africa	Polygon data containing marsh and swamp forests (*Ficus* and *Raphia* spp.), and for terrestrial classes, forests, thicket and shrub, grassland, water, and bare sand. Transformed classes were built up, timber plantations and subsistence cropland.	Used to select points for cultivated wetlands, subtropical-temperate and upland classes.	Riedel [23]
South African National Land Cover (1990, 2013/14, 2018, 2020).	A 20-m spatial resolution raster dataset containing most of the upland classes such as built-up areas, grasslands and shrublands.	To mask out transformed land cover classes, such as commercial farms and mining.	GTI [24–27]
Subsistence farming and conservation constraints in coastal peat swamp forests of the Kosi Bay Lake system, MCP, South Africa.	In-field data of floristic sampling of forested wetlands containing a classification of swamp forests as pristine, recently disturbed, old disturbed or active gardening in the Kosi Bay Forest Reserve.	Used to inform ROIs in the classification of subtropical-temperate forested wetlands and cultivated wetlands.	Grobler et al., [28]
The Vegetation Ecology of the Mfabeni Peat Swamp, St Lucia, KwaZulu-Natal.	Polygon data containing descriptions of, marsh wetlands, and forested wetlands.	Used to select subtropical-temperate forested wetland classes, large macrophytes, and marsh wetlands ROIs.	Venter [29]
Vegetation map of South Africa, Lesotho and Swaziland.	Polygon dataset including lacustrine and upland vegetation classes.	Used to inform ROIs of upland classes.	Mucina and Rutherford [30]; Dayaram et al. [6]

ROIs; these were, however, cross-checked as far as possible against imagery available in Google Earth Pro [37], which helped confirm that the ROIs still matched the landscape as it had changed over time.

Areas within historical imagery that showed no change over time were designated as reference points (Table 4). Where points fell within areas that had since been converted to other land use/land cover classes, they were either shifted to the location the wetland or land-cover type had moved to or discarded where the original wetland location could not be confirmed with confidence. This assessment drew on high-resolution historical imagery for 1990, 2000, 2006, 2014, 2018, 2020 and 2022 from Google Earth Pro [37] images (version 7.3.3.7786, covering 1985–2022) ranging between 15 cm – 15 m spatial resolution, and South African orthophotos at 50 cm spatial resolution.

Table 3
Number of field-collected points of wetland Ecosystem Functional Groups (EFGs) for each fieldwork campaign in the Maputaland Coastal Plain.

Wetland EFG name and other wetland-related classes	Description	Number of points in June 2021	Number of points in February 2022	Number of points in August 2022	Reference of the description
Burnt wetland	Desiccated peatlands with visible burn scars.	11	6	2	Grundling et al. [21]
Coastal saltmarshes	Rooted vegetation, mainly succulent chenopods found near river mouths, bays, coastal plains, and lagoons. Key species include *Atriplex patula* (Spear Saltbush / Common Orache), *Salicornia meyeriana* (Marsh Samphire), *Sarcocornia natalensis*, and *Juncus kraussii* (Dune Slack Rush), dominate these tidal systems.	0	27	3	Adams [1]; Adams et al. [31]; Lück-Vogel et al. [10]
Cultivated wetlands	A mosaic of subsistent vegetable gardens and fruit crops ranging from crops used for subsistence farming (amadumbes, cassava, maize, spinach, sugarcane, sweet potatoes, and pumpkins) to commercial farming (e.g., bananas.	10	16	4	Grobler [32]; Grobler et al. [28]
Intertidal forests and shrublands	The intertidal forests and shrublands are salt-tolerant trees, shrubs, and other plants growing in brackish to saline tidal waters. These are mostly dominated by mangrove species.	0	32	1	Keith et al. [33]
Lacustrine wetlands	Wetlands that are predominantly permanently inundated, open water bodies.	0	7	4	Keith et al. [33]
Large macrophytes	All reeds and sedges are taller than 1.5 m, including predominantly *Cyperus papyrus, Phragmites australis*, and *Typha capensis*.	22	83	4	Van Deventer et al. [34]
Marshes	Permanent and seasonal freshwater marshes or marshlands, dominated by emergent macrophytes, aerenchymatous stems and leaf tissues enable oxygen transport to roots and long rhizomes and into the substrate.	15	62	0	Keith et al. [33]; Sieben et al. [22]
Subtropical temperate forested wetlands	Forested wetlands consist of swamp, riverine, and floodplain forests. *Barringtonia racemose* (powderpuff tree), *Bridelia micrantha* (coastal golden-leaf), *Casearia glandiformis* (sword-leaf), *Cassipourea gummiflua* (Large-leaved Onionwood), *Ficus sur* (Broom Cluster Fig), *Ficus trichopoda* (Swamp Fig) are some of the key species.	28	205	9	Van Deventer et al. [18]
Total		**86**	**438**	**27**	

Step 2: Use rainfall data to identify suitable years for assessing changes in wetland EFGs

Because the maximum extent of all wetland EFGs is best captured during the wet season, this study concentrated on wet-season conditions when quantifying change. Given the sparse coverage of ground-based weather stations across the MCP, rainfall records were instead sourced from the Climate Hazards Group InfraRed Precipitation with Station data (CHIRPS [38]). Peak rainfall months were identified, with particular attention to the high-rainfall period from September to February in each composite year (Fig. 4B). Certain above-average rainfall years (e.g., 1981 and 1984; Fig. 4A) had to be excluded or adjusted because cloud cover and other image-quality issues affected the composites for those periods. Conversely, several below-average rainfall years, including 1990, 2014, 2018 and 2020, were retained because they coincide with years used in South Africa's National Land Cover products ([24–26]; 2020), which are routinely applied in ecosystem change detection and reporting for the National Biodiversity Assessments (e.g., Skowno et al. [36]). The seven years ultimately used to quantify change were therefore 1990, 2000, 2006, 2014, 2018, 2020, and 2022.

Step 3: Select and pre-process satellite data

Pre-process Landsat images

Landsat surface reflectance datasets from the Tier 1 collection in GEE [3] were used to generate image composites for 1990, 2014, and 2018 from Landsat 5, 7, and 8 images for the MCP (Fig. 5). To ensure consistency, all band names were renamed to match the bands of Landsat-8 OLI. This study used only bands common to all Landsat datasets to ensure consistency across years. The Landsat surface reflectance datasets in GEE provide calibrated surface reflectance (SR) values corrected for atmospheric effects. Additional pre-processing steps were undertaken on the Landsat surface reflectance collection in GEE for the years 1990, 2000, 2006 and 2014, using the following pre-processing steps:

- Images with $<$ 10% cloud cover were selected from the Landsat collection of images available in GEE;
- Cloudy pixels were then masked using the quality assessment (QA) bands bitmasks provided in the Landsat metadata;

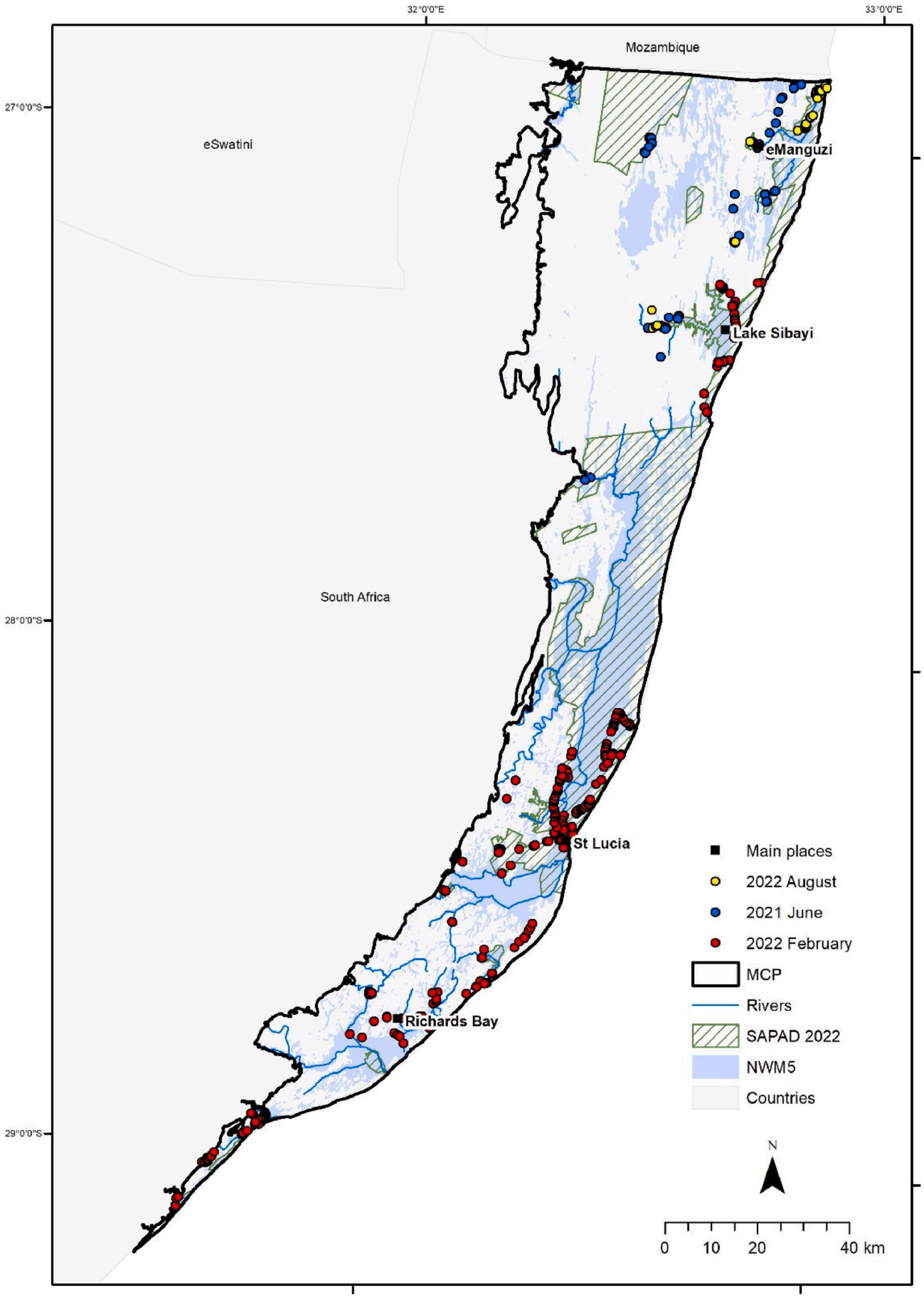

Fig. 3. Spatial distribution of the field points gathered in June 2021, February 2022 and August 2022, shown together with the Maputaland Coastal Plain boundary [18] and the South African National Protected Areas Database (SAPAD; [36]).

- The median reflectance values of the selected images were used to generate composites for the wet season of each of the seven years; and
- Finally, all the bands were scaled to reflectance values using band-dependent scaling factors available in the GEE documentation.

Imagery for 1985–1990 was too sparse and too cloud-affected to meet this study's 10% cloud-cover threshold (Fig. 5), and these

Table 4
Number of regions of interest (ROIs) selected between 1990 and 2022 for each of the wetland Ecosystem Functional Groups (EFGs) used by Keith et al. [33] and Van Deventer et al. [18]. Coding for the EFGs including F= Freshwater; MFT = Marine-Freshwater-Terrestrial; SANLC = South African National Land Cover; TF = Terrestrial-Freshwater realm.

Wetland EFG and other classes	Description	No. of ROIs 1990	No. of ROIs 2000	No. of ROIs 2006	No. of ROIs 2014	No. of ROIs 2018	No. of ROIs 2020	No. of ROIs 2022
Wetland EFGs								
Coastal Saltmarshes (MFT1.3)	Coastal saltmarshes comprise rooted vegetation, mainly succulent chenopods found near river mouths, bays, coastal plains, and lagoons.	366	421	349	366	358	366	367
Intertidal forests and shrublands (MFT1.2)	The Intertidal forests and shrublands are salt-tolerant trees, shrubs, and other plants growing in brackish to saline tidal waters. These are mostly dominated by mangrove species.	938	890	879	938	938	938	939
Lacustrine wetlands (F1 and F2)	Open water bodies, including large lakes and river channels.	581	359	554	538	512	348	575
Large macrophytes (TF.8)	All reeds and sedges are taller than 1.5 m, including predominantly *Cyperus papyrus, Phragmites australis*, and *Typha capensis*. Added to the classification due to abundance and separability as the 8th class in the TF realm.	2 951	1 574	2 360	2 613	2 608	2 851	2 951
Seasonal and permanent marshes (TF1.3 and TF1.4)	Permanent and seasonal freshwater marshes or marshlands, dominated by emergent macrophytes, aerenchymatous stems, and leaf tissues enable oxygen transport to roots and long rhizomes and into the substrate.	1 042	1 112	957	1 112	1 133	1 106	1 043
Subtropical - temperate forested wetlands (TF1.2)	Forested wetlands consist of swamp, riverine, and floodplain forests.	917	941	941	941	905	938	917
Terrestrial ecosystem types								
Bare land	Dryland consists of sand or soil with no vegetation cover.	922	201	543	676	526	1 019	922
Beach	Coastal landforms alongside seawater consist of loose particles, typically made from rock, such as sand, gravel, and pebbles.	785	777	758	798	784	796	784
Coastal forests	Lowland terrestrial forests along the Indian Coastal Belt, including species such as the Flat-crown (*Albizia adianthifolia*), coastal golden leaf (*Bridelia micrantha*), red beech (*Protorhus longifolia*), forest mahogany (*Trichilia dregeana*) and forest fever-berry (*Croton sylvaticus*).	1 967	1 821	2 054	2 156	1 841	2 156	1 967
Dune forests	A rich vegetation community comprising a variety of trees, shrubs, and herbaceous plants, many of which have adapted to the sandy, nutrient-poor soils [6].	736	593	593	593	593	593	580
Sand forests	Subtropical forest regions with unique restrictions on ancient coastal dunes.	780	331	331	331	331	331	305
Shrubs	Small-to-medium-sized woody plants.	690	751	741	752	707	707	690
Terrestrial grasses	Large open areas of dry grass.	963	812	963	974	974	955	963
Anthropogenically transformed land use/land cover classes								
Built-up	Areas dominated by human-made structures, such as buildings and roads.	870	1 718	629	790	887	887	784
Burnt peatland	Peatland areas that have experienced fire events, with visible burn scars.	142	0	0	82	82	106	142
Cleared land	Areas where vegetation and other obstacles have been removed, typically for construction or agricultural purposes, leaving soil exposed.	736	262	316	344	599	706	736
Commercial farms	Large-scale farming operations focused on the production of crops, mainly maize, sugarcane and pineapple stands.	780	676	738	761	780	780	780
Cultivated wetlands	A mosaic of subsistence vegetable gardens and fruit crops ranging from crops used for subsistence farming (amadumbes, cassava, maize, spinach, sugarcane, sweet potatoes, and pumpkins) to commercial farming.	492	63	79	395	472	492	492

(continued on next page)

Table 4 (*continued*)

Wetland EFG and other classes	Description	No. of ROIs 1990	No. of ROIs 2000	No. of ROIs 2006	No. of ROIs 2014	No. of ROIs 2018	No. of ROIs 2020	No. of ROIs 2022
Relic gardens	Historical wetland gardens are often associated with indigenous cultivation practices.	256	256	245	257	256	256	257
Timber plantations	Large-scale timber plantations. This includes both commercial and subsistence timber plantations.	3 701	1 355	1 570	974	256	3 099	963
Total		**20 615**	**14 913**	**15 600**	**16 391**	**1 542**	**19 430**	**17 157**

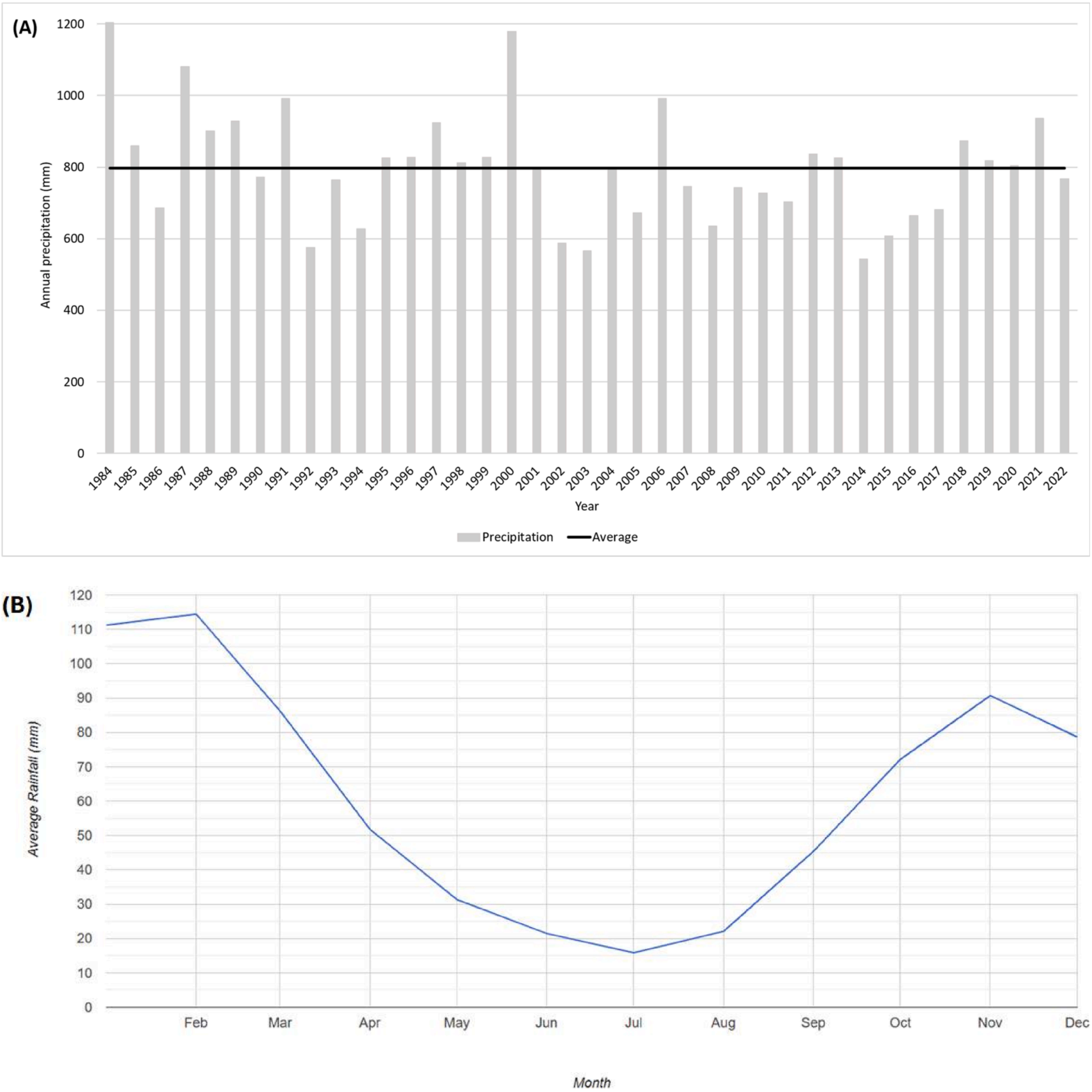

Fig. 4. Rainfall in the Maputaland Coastal Plain, with (a) average precipitation data between 1981 and 2022 from the Climate Hazards Group InfraRed Precipitation with Station data (CHIRPS; [38]), where the black line indicates the average rainfall across this period; and (b) average rainfall for each month between 1981 and 2022 derived from the CHIRPS data.

years were therefore excluded from the classification. To address possible data gaps arising from the Landsat 7 Scan Line Corrector (SLC) failure affecting scenes acquired after May 2003, a median composite combining overlapping Landsat 5 TM and Landsat 7 ETM+ scenes was used; wherever the two sensors overlapped, this approach filled the SLC-off gaps and produced full coverage of the study area.

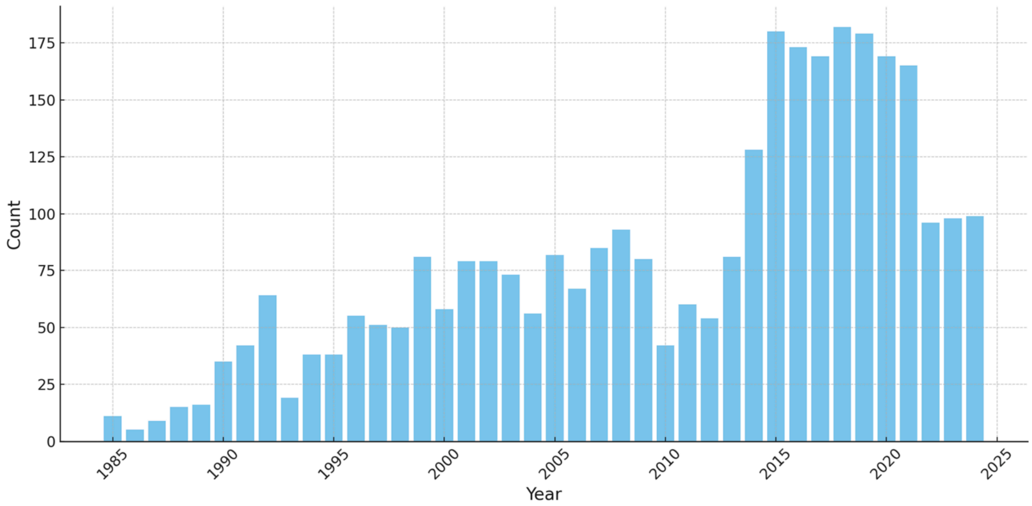

Fig. 5. Availability of Landsat data between 1985 and 2024 in GEE for the Maputaland Coastal Plain.

Pre-process Sentinel-1 and −2 images

Sentinel-1 is a European Space Agency (ESA) C-band synthetic aperture radar (SAR) mission pair operating primarily in interferometric wide-swath (IW) mode with a nominal six-day revisit. Following the loss of Sentinel-1B in December 2021, only Sentinel-1A remained operational, extending the revisit interval to 12 days. Dual-polarimetric (VV and VH) ground-range detected (GRD) scenes, calibrated and orthorectified at 10–40 m spatial resolution, are available in GEE. Pre-processing of the Sentinel-1 data followed the approach of Mullissa et al. [39], covering scene selection, noise correction, speckle filtering and terrain normalization.

Sentinel-2, on the other hand, is a two-satellite constellation (S2A and S2B) operated by ESA, offering a 90 km swath width [40]. Its 12 spectral bands are delivered at 10 m, 20 m and 60 m resolution. This study used GEE's Level-2A Sentinel-2 surface reflectance product, atmospherically corrected with the Sen2Cor v2.11 algorithm and default location-based parameters [41,42]. Sen2Cor derives surface reflectance from scene metadata and auxiliary information, such as atmospheric profiles and aerosol optical thickness [42]. Pixels affected by cloud or cloud shadow were removed using the built-in QA60 band, and scenes were additionally filtered to retain only those with 10% cloud cover or less.

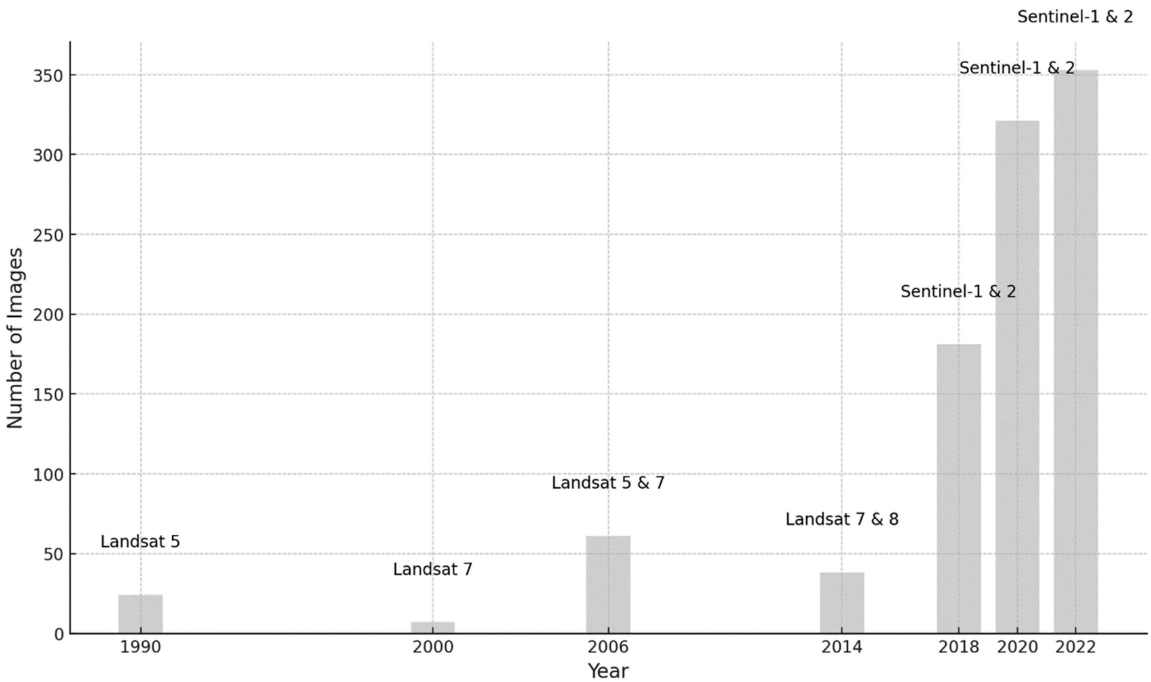

Fig. 6. The number of images and sensors used for each composite year between 1990 and 2022.

Within GEE, the Sentinel-1 and Sentinel-2 scenes were merged into composites, combining bands from both datasets at a common 10 m spatial resolution. The number of images contributing to each composite year is shown in Fig. 6.

Step 4: Calculate spectral indices and other datasets to enhance variable importance selection and classification accuracies

Elevation, vegetation, and water-related datasets were derived to supplement the landscape information available for wetland mapping (Table 5). Elevation data, used to assess the likely direction of water flow and accumulation, are important predictors of wetland distribution and function [43] and were used in GEE to derive elevation, slope, and aspect layers. Vegetation indices helped distinguish the different vegetation types that characterise wetland ecosystems. Water indices, which are central to characterizing wetlands [44] were included to capture the extent of open water and soil moisture. Topographic indices, including the topographic wetness index (TWI) and topographic position index (TPI), provided additional information on landforms and the movement of water across the landscape [45,46]. Texture indices were also derived to capture spatial patterns and variation in surface materials, aiding differentiation between wetland types. These texture indices required a simulated grayscale panchromatic band for both the Landsat and Sentinel-2 imagery, computed as a linear combination of the green, near-infrared (NIR), and red bands using Equations 1 and 2.

Equation 1: Simulated panchromatic band from Sentinel-2 bands

$$\mathrm{PAN\_S2} = (0.3 \times \mathrm{NIR}) + (0.59 \times \mathrm{red}) + (0.11 \times \mathrm{green})$$

Equation 2: Simulated panchromatic band from Landsat-5 bands

$$\mathrm{PAN\_L} = (0.52 \times \mathrm{NIR}) + (0.23 \times \mathrm{red}) + (0.25 \times \mathrm{green})$$

Here, PAN_S2 denotes the panchromatic image derived from Sentinel-2, PAN_L the equivalent derived from Landsat, and the coefficients reflect the weighting of each band's contribution [55]. A Principal Component Analysis (PCA) was then run on the 36 Gray-Level Co-Occurrence Matrix (GLCM) texture features generated from these panchromatic bands for the respective Landsat and Sentinel-2 sensors, retaining only the first three Principal Components, which together explained 90–95% of the variance. Before classification, feature selection and optimization were performed using the recursive feature elimination (RFE) algorithm [56] in R (version 2023.03.1; R Team, 2023), with the 'caret' package [57]. RFE automatically identifies the most influential variables (the top 20, in this case) within a dataset and was run here with cross-validation.

Step 5: Classify wetland EFGs

Wetland EFG types were classified in GEE using the Random Forest classification algorithm [58], an ensemble method that combines many decision trees to increase classification accuracy and robustness. The number of trees was set to 1000, and *mtry* was left at its default (the square root of the number of predictor variables). Training data were split randomly into 70% for model training and 30% for testing. Raster outputs were generated at 30 m spatial resolution for the years 1990, 2000, 2006 and 2014, and at 10 m spatial resolution for 2018, 2020 and 2022. A confusion matrix was used to compute overall, user and producer accuracy [59].

Table 5
Spectral and radar indices that were included in the classification of wetland Ecosystem Functional Groups (EFGs). NIR = near-infrared; SWIR = Shortwave infrared.

Spectral index	Equation	Wetland EFG property enhanced
Difference Vegetation Index (DVI); Tucker [47]	$DVI = NIR - Red$	Soil Moisture
Enhanced Vegetation Index (EVI) [48,49])	$EVI = 2.5 \times \frac{(NIR - Red)}{(NIR + (6 \times Red - 7.5 \times Blue) + 1}$	Chlorophyll
Green Difference Vegetation Index (GDVI); Tucker et al. [50]	$GDVI = NIR - Green$	Chlorophyll and nitrogen
Green Normalized Difference Vegetation Index (GNDVI); Gitelson et al. [51]	$gNDVI = \frac{(NIR - Green)}{(NIR + Green)}$	Chlorophyll
Green Soil Adjusted Vegetation Index (GSAVI); Mahdianpari et al. [44]	$gSAVI = \frac{(NIR - Green)}{(NIR + Green)} \times 1.5$	Chlorophyll
Modified Normalised Difference Water Index (MNDWI) [46]	$MNDWI = \frac{(Green - SWIR)}{(Green + SWIR)}$	Leaf water content
Modified Soil Adjusted Vegetation Index (MSAVI); Qi et al. [52]	$MSAVI = \frac{2NIR + 1 - \sqrt{(2NIR+1)^2 - 8(NIR - RED)}}{2}$	Chlorophyll
Normalised Difference Vegetation Index (NDVI); Tucker [47]	$NDVI = \frac{(NIR - Red)}{(NIR + Red)}$	Chlorophyll
Normalised Difference Water Index (NDWI) [53]	$NDWI = \frac{(RNIR - RSWIR)}{(RNIR + RSWIR)}$	Leaf water content
Optimised Soil Adjusted Vegetation Index (OSAVI) [54]	$OSAVI = \frac{(NIR - Green)}{(NIR + Red) + 0.16}$	Chlorophyll and leaf area index
Red Edge Normalized Difference Vegetation Index (NDVIre) [51]	$NDVIre = \frac{(NIR - Red\ Edge)}{(NIR + Red\ Edge)}$	Chlorophyll, leaf area/biomass and nitrogen
Sentinel-1 ratio [12]	$Sratio = \frac{VV}{VH}$	Vegetation structure and vegetation inundation

Step 6: Classify seasonal and permanent marshes

Because Seasonal and Permanent marshes share similar spectral and radar backscatter signatures during wet periods, when both are saturated, these two classes were initially treated as a single combined marsh class. This combined class was later separated from the broader classification for each composite. For each composite year, the normalised difference water index (NDWI; [53,60]) was tracked across the full composite period, monthly where possible, and at three-month intervals for 1990 and 2000, given the limited availability of monthly imagery in those years. NDWI serves as a proxy for wetland inundation: dry conditions typically correspond to NDWI values below −0.3, while values above −0.2 indicate saturation or inundation [61]. Variation in NDWI across a wetland area over time therefore indicates how frequently that area experiences standing water. Based on this NDWI-derived water-occurrence frequency for each year, marshes were classified as follows:

- Permanent marshes: inundated for >80% of the year [12].
- Seasonal marshes: inundated between 20% and 80% of the year [12].
- Ephemeral marshes: inundated for 20% or less of the year.

Step 7: Calculate the extent of changes in wetland EFGs

To quantify the extent of each wetland EFG classification, all maps were reprojected to South Africa's AEA coordinate system. The area occupied by each EFG was then calculated in km^2, along with the proportion each EFG represented relative to the overall MCP area. Results are reported both as the absolute extent of each wetland EFG and as a percentage of the total MCP extent.

Step 8: Determine areas where wetland transitions took place and hotspot areas of change

A change matrix was used to identify transitions between aquatic and terrestrial classes, estuarine and freshwater classes, and the loss of forested wetland to Large macrophytes or marsh, as well as wetlands that remained stable and changes attributable to spectral confusion. This analysis was carried out in ArcGIS Pro 3.0 [62] using the Compute Change Raster tool with the categorical difference parameter.

Step 9: Calculate rates of change in EFGs

The rate of change for each class was calculated via Equation 3 [63].

Equation 3: Rate of change [63]:

$$r = \left(\frac{1}{t2 - t1}\right) \times ln\left(\frac{a2}{a1}\right)$$

In this equation, r is the average rate of change and ln denotes the natural logarithm. This formulation captures how much a quantity grows or declines between an initial value a1 at time t1 and a final value a2 at time t2.

Step 10: Calculate absolute rate of decline

The absolute rate of decline (ARD) was calculated for each wetland EFG to project the year at which the ecosystem would reach 100% decline [64], following Equation 4.

Equation 4: Absolute rate of decline [64]:

$$ARD = \frac{Area\ (t2)\ -\ Area\ (t1)}{t2\ -\ t1}$$

$Area\ (t2)$ and $Area\ (t1)$ are the measured areas at the initial and final time steps, respectively. The ARD was projected over a 50-year window, from 2000 to 2050. The year 2000 was chosen as the baseline for classifying wetland EFGs in the MCP because it represents a meaningful benchmark for recent ecological conditions [18]: it followed the highest rainfall recorded in KwaZulu-Natal Province in eight decades, driven by the extensive flooding associated with Cyclone Eline [65]. The wetland extent recorded after this extreme event closely reflected the wetlands' natural state in recent times, making 2000 a dependable reference point for tracking subsequent change [66;18].

Step 11: Accuracy assessment and method validation

The success of the method was evaluated and tested in three ways: a statistical accuracy assessment based on held-out reference points, a spatial comparison against fine-scale, ground-validated maps in selected regions of the MCP, and a comparison of this study's user accuracies against other published wetland datasets covering the MCP.

Statistical accuracy assessment

For each classification year, the field and ancillary reference points were split randomly, with 70% used to train the classifier and

30% withheld to build a confusion matrix in Google Earth Engine using the ee.ConfusionMatrix() function. Three metrics were calculated from each matrix: overall accuracy, user's accuracy, and producer's accuracy.

The overall accuracy of a classification provides a general measure of how well the classification process performed in correctly identifying different wetland EFGs [59]. It is the percentage of correctly classified pixels in relation to the total number of pixels (Equation 5).

Equation 5: Overall Accuracy (OA)

$$OA = \frac{Sum\ of\ major\ diagonal}{Sum\ of\ total\ correct\ pixels} x100$$

The user's accuracy, also known as the error of commission, indicates the likelihood that a pixel classified into a certain category represents that category on the ground EFGs (Equation 6; [59]). Users who rely on the classification must understand the probability that a given area is correctly identified as a wetland EFG.

Equation 6: User accuracy (UA)

$$\mathrm{UA} = \frac{\text{Total number of correct pixels in a category}}{\text{row total}}$$

The producer's accuracy, or the error of omission, reflects the probability of a certain ground truth category being correctly classified as an EFG (Equation 7; [59]). This metric is important because producers of the classification need to measure how well the classification algorithm has performed on individual wetland classes mapped.

Equation 7: Producer accuracy (PA)

$$PA = \frac{Total\ number\ of\ corect\ pixels\ in\ a\ category}{column\ total}$$

Spatial comparison against fine-scale, ground-validated maps

The classified outputs were compared to two maps that were independent of this study's training data, both produced through ground-validated heads-up digitisation at a spatial resolution considerably finer than the Landsat or Sentinel classifications. The first compared this study's 2006 Landsat classification to Venter [29], who digitised wetland EFGs in the uMfabeni Peatland in the MCP from a mosaic of colour aerial photography at 23 cm spatial resolution using ground-validated heads-up digitisation. Raster outputs for the uMfabeni Peatland were converted to polygons and overlaid with Venter's [29] polygons for the Large macrophytes, Marsh wetlands, and Subtropical-temperate forested wetlands classes, and the area (km^2) mapped by each dataset was compared to calculate a percentage agreement per class. The second compared this study's 2018 classification, produced from Sentinel-1 and Sentinel-2 imagery, to the estuarine wetland EFG map of Adams et al. [67], who mapped coastal saltmarshes and intertidal forests and shrublands along the estuarine functional zone of the MCP using heads-up digitisation of Google Earth Pro [37] imagery and aerial photographs spanning 2008 to 2018. The same overlay and percentage-agreement procedure was applied to these two classes.

Comparison against other published wetland datasets

User's accuracies from this study's Landsat classifications (1990, 2000, 2006 and 2014) were compared with those reported for the same wetland EFGs by three other datasets covering the MCP or a wider area: the South African National Land Cover of 2014 (SANLC2014), the South African coastal ecosystem map of Bessinger et al. [7], and the Global Annual Wetland Dataset [68]. We also compared against the continental African wetland dataset of Li et al. [69], which used Landsat imagery and a random forest classifier, closely matching this study's approach for direct comparison.

The method presented here was applied to support the RLE and the associated rate-of-change assessment in Van Deventer et al. [4]. Relative to other datasets that also mapped some or all of the six wetland EFGs, this method produced a more accurate mapping of the extent of all six EFGs than fine-scale, in-field delineation carried out by botanists (see the Discussion and Supplementary Information in [4,29]). While the workflow and GEE environment could reasonably be extended to other study areas, its success here owes much to the thorough desktop and, in particular, field data collection, which was carefully designed to capture change over time. The time and cost invested in validation, therefore, contribute substantially to the representativeness and accuracy of the outputs.

Limitations

The limited availability of historical Landsat data constrained the temporal scope of this analysis and may have limited a fuller assessment of long-term EFG trends. Imagery from the 1980s was scarce and largely too cloud-affected to allow whole-study-area composites to be generated. The relatively coarse spatial resolution of the older imagery can also lead to overestimation of the extent of EFGs that are narrow or small: where a wetland covers >60% of a pixel, the entire pixel is assigned to that class, which can inflate extent estimates in years relying on Landsat imagery relative to years using Sentinel data. Further work is needed to quantify the error associated with the Landsat-based years and to assess whether this error could be corrected retrospectively for red list assessments of these ecosystems.

In addition, the sparse coverage of the South African Weather Service's rainfall gauges across the study area made it necessary to rely on CHIRPS data, which, although useful, may not fully reflect local rainfall patterns. Future work could focus on areas experiencing substantial anthropogenic change to characterise the degree of degradation.

Ethics statements

This study did not involve human participants, animal experimentation, or data sourced from social media. Fieldwork was carried out within the study area described above, with appropriate permission obtained from the Mbasa and Tembe Traditional Councils, who granted access to work on their land, as well as from the iSimangaliso Wetland Park Authority and Ezemvelo KwaZulu-Natal Wildlife (EKZNW), South Africa who authorised sampling within the protected areas of the study region. No harm was caused to any person, animal or wildlife during this fieldwork.

CRediT author statement

Philani Apleni: Writing, Writing original draft, Methodology, Software, Formal analysis, Investigation. **Heidi Van Deventer:** Conceptualisation, Funding acquisition, Project administration, Supervision, Writing – review & editing, Investigation. **Laven Naidoo**: Conceptualisation, Supervision, Writing – review & editing. **Philemon Tsele**: Supervision, Writing – review & editing.

Declaration of competing interest

The authors declare the following financial interests/personal relationships, which may be considered as potential competing interests: *Please declare any financial interests/personal relationships which may be considered as potential competing interests here.*

During the preparation of this work, the author(s) used the free version of Grammarly to check and correct the English language. After using this tool/service, the author(s) reviewed and edited the content as needed and take full responsibility for the content of the published article.

Acknowledgements

The Council for Scientific and Industrial Research (CSIR) and the Water Research Commission (C2020-2021-000427) provided funding for the report. The Mbasa and Tembe Traditional Councils were crucial in allowing us to work on their territory, and for that we are grateful. We also thank Ezemvelo KwaZulu-Natal Wildlife (EKZNW) and the iSimangaliso Wetland Park Authority for allowing us to sample in their respective protected areas. We also thank Dr. Piet-Louis Grundling for taking the time to show us significant locations on the MCP and for introducing us to the subject of wetlands in general. Additionally, Dr. Althea Grundling, Ms. Susan Janse van Rensburg, Mr. Siphiwe Mfeka, Dr. Wouter le Roux and Mr Retief Grobler.

Data availability

https://doi.org/10.71506/csirza.32006340 (The data can be downloaded from here: .)

References

[1] J.B. Adams, Salt marsh at the tip of Africa: patterns, processes and changes in response to climate change, Estuar. Coast. Shelf Sci. 237 (2020) 106650, https://doi.org/10.1016/j.ecss.2020.106650.
[2] D.A. Keith, J.R. Ferrer-Paris, E. Nicholson, R.T. Kingsford, IUCN Global Ecosystem Typology 2.0. Descriptive profiles For Biomes and Ecosystem Functional Groups, International Union for Conservation of Nature, 2020, https://doi.org/10.2305/IUCN.CH.2020.13.en.
[3] N. Gorelick, M. Hancher, M. Dixon, S. Ilyushchenko, D. Thau, R. Moore, Google Earth Engine: planetary-scale geospatial analysis for everyone, Remote Sens. Environ. 202 (1) (2017) 18–27, https://doi.org/10.1016/j.rse.2017.06.031. https://www.sciencedirect.com/science/article/pii/S0034425717302900. Data DOI.
[4] H. Van Deventer, P. Apleni, L. Naidoo, P. Tsele, Quantifying the Extent and Rates of Change in Wetland Ecosystem Functional Groups in the Maputaland Coastal Plain of South Africa, STOTEN, 2026.
[5] H. Van Deventer, L. Van Niekerk, J. Adams, M.K. Dinala, R. Gangat, S.J. Lamberth, M. Lötter, N. Mbona, F. Mackay, J.L. Nel, C.L. Ramjukadh, A. Skowno, S. P. Weerts, National wetland map 5: an improved spatial extent and representation of inland aquatic and estuarine ecosystems in South Africa, Water SA 46 (1) (2020) 66–79, https://doi.org/10.17159/wsa/2020.v46.i1.7887.
[6] A. Dayaram, L.R. Harris, B.A. Grobler, S. van der Merwe, A.G. Rebelo, L.W. Powrie, J.H.J. Vlok, P.G. Desmet, M. Qabaqaba, K.M. Hlahane, A.L. Skowno, Vegetation Map of South Africa, Lesotho and Swaziland 2018: a description of changes since 2006, Afr. Biodivers. Conserv. 49 (1) (2019) 1–11, https://doi.org/10.4102/abc.v49i1.2452.
[7] M. Bessinger, M. Lück-Vogel, A. Skowno, F. Conrad, Landsat-8 based coastal ecosystem mapping in South Africa using random forest classification in Google Earth Engine, S. Afr. J. Bot. 150 (2022) 928–939, https://doi.org/10.1016/j.sajb.2022.08.014.
[8] M. Dlamini, E. Adam, G. Chirima, H. Hamandawana, A remote sensing-based approach to investigate changes in land use and land cover in the lower uMfolozi floodplain system, South Africa, Trans. R. Society South Africa 76 (1) (2021) 13–25.
[9] A.T. Grundling, E.C. Van Den Berg, J.S. Price, Assessing the distribution of wetlands over wet and dry periods and land-use change on the Maputaland Coastal Plain, north-eastern KwaZulu-Natal, South Africa, SA JoG 2 (2) (2013). https://sajg.org.za/index.php/sajg/article/view/84.
[10] M. Lück-Vogel, C. Mbolambi, K. Rautenbach, J. Adams, L. Van Niekerk, Vegetation mapping in the St Lucia estuary using very high-resolution multispectral imagery and LiDAR, SAJB 107 (2016) 188–199, https://doi.org/10.1016/j.sajb.2016.04.010.
[11] M. Ramjeawon, M. Demlie, M.L. Toucher, S. Janse Van Rensburg, Analysis of three decades of land cover changes in the Maputaland Coastal Plain, South Africa. Koedoe 62 (1) (2020) a1642, https://doi.org/10.4102/koedoe.v62i1.1642.
[12] B. Slagter, N.E. Tsendbazar, A. Vollrath, J. Reiche, Mapping wetland characteristics using temporally dense Sentinel-1 and Sentinel-2 data: a case study in the St. Lucia wetlands, South Africa, Int. J. Appl. Earth Obs. Geoinf. 86 (2020) 102009, https://doi.org/10.1016/j.jag.2019.102009.
[13] H. Van Deventer, M.A. Cho, O. Mutanga, Improving the classification of six evergreen subtropical tree species with multi-season data from leaf spectra simulated to WorldView-2 and RapidEye, IJRS 38 (17) (2017) 4804–4830, https://doi.org/10.1080/01431161.2017.1320445.

[14] H. Van Deventer, M.A. Cho, O. Mutanga, Multi-season RapidEye imagery improves the classification of wetland and dryland communities in a subtropical coastal region, ISPRS J. Photogramm. Remote Sens. 157 (2019) 171–187, https://doi.org/10.1016/j.isprsjprs.2019.09.007.
[15] M.L. Pretorius, in: L.R. Brown, G.J. Bredenkamp, C. van Huyssteen (Eds.), A Vegetation classification and Description of Five Wetland Systems and Their Respective Zones on the Maputaland Coastal Plain, Environmental Management]. University of South Africa, Pretoria, South Africa, 2012.
[16] M.A. Cho, O. Malahlela, A. Ramoelo, Assessing the utility WorldView-2 imagery for tree species mapping in South African subtropical humid forest and the conservation implications: DukuDuku Forest patch as case study, Int. J. Appl. Earth Observ. Geoinform. 38 (2015) 349–357, https://doi.org/10.1016/j.jag.2015.01.015.
[17] M.A. Cho, A. Ramoelo, P. Debba, O. Mutanga, R. Mathieu, H. Van Deventer, N. Ndlovu, Assessing the effects of subtropical forest fragmentation on leaf nitrogen distribution using remote sensing data, Landsc. Ecol. 28 (8) (2013) 1479–1491.
[18] H. Van Deventer, J.B. Adams, J.F. Durand, R. Grobler, P.L. Grundling, S. Janse van Rensburg, D. Jewitt, B. Kelbe, C.F. MacKay, L. Naidoo, J.L. Nel, L. Pretorius, T. Riddin, L. Van Niekerk, Conservation conundrum – red listing of subtropical-temperate coastal forested wetlands of South Africa, Ecol. Indic. 130 (2021) 108077, https://doi.org/10.1016/j.ecolind.2021.108077.
[19] Arndt J. (2014) Distribution and long-term historic impact of the small-scale subsistence farming on wetlands in the Maputaland, KwaZulu-Natal (South Africa). MSc thesis, Technische Universitat Munchen, Berlin, Germany.
[20] A.P. Starke, C.J. Geldenhuys, T.G. O'Connor, C.S. Everson, Forest and woodland expansion into forestry plantations informs screening for native agroforestry species, Maputaland South Africa, Forests, Trees Livelihoods 29 (1) (2020) 1–15, https://doi.org/10.1080/14728028.2019.1670740.
[21] P.L. Grundling, A.T. Grundling, H. Van Deventer, J.P. Le Roux, Current state, pressures and protection of South African peatlands, Mires Peat 27 (2021) 26. http://doi.org/10.19189/map.2020.omb.sta.2125.
[22] E.J.J. Sieben, T. Nyambeni, H. Mtshali, F.T.J. Corry, C.E. Venter, D.R. MacKenzie, T.E. Matela, L. Pretorius, D.C. Kotze, The herbaceous vegetation of subtropical freshwater wetlands in South Africa: classification, description and explanatory environmental factors, S. Afr. J. Bot. 104 (2016) 158–166, https://doi.org/10.1016/j.sajb.2015.11.005.
[23] M. Riedel, J. Sliva, T. Schneider, N. Guerrero, J. Kollmann, Development of land-cover classification focusing on wetlands impacted by subsistence farming using satellite remote sensing, in: Proceedings of Tropentag 2015: Conference on international research on food security, natural resource management and rural development, Humboldt-Universität zu Berlin & Leibniz Centre for Agricultural Landscape Research (ZALF), Berlin, Germany, 2015. https://www.tropentag.de/2015/abstracts/full/1029.pdf.
[24] GeoTerraImage (GTI) Pty Ltd., 1990 South African National land-Cover dataset. DEA/CARDNO SCPF002: implementation of land-use 626 maps for South Africa. Project Specific Data User Report and Metadata version 05, South African Department of Environment Forestry and 627 Fisheries (DFFE), Pretoria, South Africa, 2015. http://egis.environment.gov.za.
[25] GeoTerraImage (GTI) Pty Ltd., The 2013-2014 South African National land-Cover Dataset, 2013-14 SA Landcover report. Contents 629 Version 05 (DEA Open access). Data User Report and Metadata, South African Department of Environment Forestry and Fisheries (DFFE), Pretoria, South Africa, 2015. http://egis.environment.gov.za.
[26] GeoTerraImage (GTI) Pty Ltd., 2018 South African national Land Cover Dataset Version 4, South African Department of Environment Forestry and Fisheries (DFFE), Pretoria, South Africa, 2019. http://egis.environment.gov.za.
[27] GeoTerraImage (GTI) Pty Ltd., 2020 South African national Land Cover Dataset, South African Department of Environment Forestry and 634 Fisheries (DFFE), Pretoria, South Africa, 2021. http://egis.environment.gov.za.
[28] R. Grobler, C. Moning, J. Sliva, G. Bredenkamp, P.-L. Grundling, Subsistence farming and conservation constraints in coastal peat swamp forests of the Kosi Bay Lake system, Maputaland, South Africa, Géocarrefour 79 (4) (2004) 317–324, https://doi.org/10.4000/geocarrefour.842.
[29] C.E. Venter, in: G.J. Bredenkamp (Ed.), The Vegetation Ecology of Mfabeni peat swamp, St Lucia, KwaZulu-Natal, [Magister Scientia]. University of Pretoria, Hatfield, South Africa, 2003.
[30] L. Mucina, M.C. Rutherford (Eds.), The Vegetation of South Africa, Lesotho and Swaziland. Strelitzia 19, South African National Biodiversity Institute, Pretoria, South Africa, 2006.
[31] J.B. Adams, D. Veldkornet, P. Tabot, Distribution of macrophyte species and habitats in South African estuaries, S. Afr. J. Bot. 107 (2016) 5–11, https://doi.org/10.1016/j.sajb.2016.08.001.
[32] L.E.R. Grobler, A phytosociological study of peat swamp forests in the Kosi Bay lake system. Maputaland, South Africa [Magister Scientiae], University of Pretoria, South Africa, 2009. https://repository.up.ac.za/items/60220dc1-6a44-499f-bbf8-7c5581008af1.
[33] D.A. Keith, J.R. Ferrer-Paris, E. Nicholson, M.J. Bishop, B.A. Polidoro, E. Ramirez-Llodra, M.G. Tozer, J.L. Nel, R. Mac Nally, E.J. Gregr, K.E. Watermeyer, F. Essl, D. Faber-Langendoen, J. Franklin, C.E.R. Lehmann, A. Etter, D.J. Roux, J.S. Stark, J.A. Rowland, R.T. Kingsford, A function-based typology for Earth's ecosystems, Nature 610 (7932) (2022) 513–518, https://doi.org/10.1038/s41586-022-05318-4.
[34] H. Van Deventer, A. Linström, L. Naidoo, N. Job, E.J.J. Sieben, M.A. Cho, Comparison between Sentinel-2 and WorldView-3 sensors in mapping wetland vegetation communities of the Grassland Biome of South Africa, for monitoring under climate change, RSASE 28 (2022) 100875, https://doi.org/10.1016/j.rsase.2022.100875.
[35] J.P. Snyder, Map Projections – a Working Manual, United States Government Printing Office, 1987.
[36] A.L. Skowno, C.J. Poole, D.C. Raimondo, K.J. Sink, H. Van Deventer, L. Van Niekerk, L.R. Harris, L.B. Smith-Adao, K.A. Tolley, T.A. Zengeya, W.B. Foden, G. F. Midgley, A. Driver. South African National Biodiversity Institute, An Entity of the Department of Environment, Forestry and Fisheries, Pretoria, National Biodiversity Assessment 2018: The Status of South Africa's Ecosystems and Biodiversity. Synthesis Report, 2019. http://hdl.handle.net/20.500.12143/6362.
[37] Google Earth Pro (GEP), GEP Version 7.3.3.7786, Various images Composites Available in GEP For the Estuarine Functional Zones of South Africa, –2002, the server kh.google.com, 1985. Available fromand, http://www.earth.google.com.
[38] C. Funk, P. Peterson, M. Landsfeld, D. Pedreros, J. Verdin, S. Shukla, G. Husak, J. Rowland, L. Harrison, A. Hoell, J. Michaelsen, The climate hazards infrared precipitation with stations—a new environmental record for monitoring extremes, Sci. Data. 2 (2) (2015) 150066, https://doi.org/10.1038/sdata.2015.66.
[39] A. Mullissa, A. Vollrath, C. Odongo-Braun, B. Slagter, Sentinel-1 SAR backscatter analysis ready data preparation in Google Earth Engine, Remote Sens. 13 (10) (2021) 1954, https://doi.org/10.3390/rs13101954.
[40] M. Drusch, U. Del Bello, S. Carlier, O. Colin, V. Fernandez, F. Gascon, P. Bargellini, Sentinel-2: ESA's optical high-resolution mission for GMES operational services, Rem. Sens. Env. 120 (2012) 25–36, https://doi.org/10.1016/j.rse.2011.11.026.
[41] European Space Agency (ESA), Sen2Cor v2.11, European Space Agency, 2022. https://step.esa.int/main/snap-supported-plugins/sen2cor/sen2cor-v2-11/. accessed 21 January 2025.
[42] M. Main-Knorn, B. Pflug, J. Louis, V. Debaecker, U. Müller-Wilm, F. Gascon, in: Sen2Cor for Sentinel-2". Proc. SPIE 10427, Image and Signal Processing for Remote Sensing XXIII, 2017 1042704. http://www.doi.org/10.1117/12.2278218.
[43] J.R.B. Bwangoy, M.C. Hansen, D.P. Roy, G. De Grandi, C.O. Justice, Wetland mapping in the Congo Basin using optical and radar remotely sensed data and derived topographical indices, Remote Sens. Env. 114 (1) (2010) 73–86, https://doi.org/10.1016/j.rse.2009.08.004.
[44] M. Mahdianpari, H. Jafarzadeh, J.E. Granger, F. Mohammadimanesh, B. Brisco, B. Salehi, S. Homayouni, Q. Weng, A large-scale change monitoring of wetlands using time series Landsat imagery on Google Earth Engine: a case study in Newfoundland, GISci. Remote Sens. 57 (8) (2020) 1102–1124, https://doi.org/10.1080/15481603.2020.1846948.
[45] K.J. Beven, M.J. Kirkby, A physically based, variable contributing area model of basin hydrology */un modèle à base physique de zone d'appel variable de l'hydrologie du bassin versa*nt, Hydrolog. Sci. Bull., 24 24 (1979) 43–69, https://doi.org/10.1080/02626667909491834.
[46] A. Weiss, Topographic position and landforms analysis, in: Poster Presentation, ESRI User Conference 200, The Nature Conservancy (TNC), Northwest Division, 2001, p. 1. https://env761.github.io/assets/files/tpi-poster-tnc-18x22.pdf.
[47] C.J. Tucker, Red and photographic infrared linear combinations for monitoring vegetation, Remote Sens. Environ. 8 (2) (1979) 127–150, https://doi.org/10.1016/0034-4257(79)90013-0.

[48] A. Huete, C. Justice, H. Liu, Development of vegetation and soil indices for MODIS-EOS, Remote Sens. Environ. 49 (3) (1994) 224–234, https://doi.org/10.1016/0034-4257(94)90018-3.
[49] A. Huete, K. Didan, T. Miura, E.P. Rodriguez, X. Gao, L.G. Ferreira, Overview of the radiometric and biophysical performance of the MODIS vegetation indices, Remote Sens. Environ 83 (1) (2002) 195–213. http://www.doi.org/10.1016/S0034-4257(02)00096-2.
[50] C.J. Tucker, J.H. Elgin, J.E. McMurtrey, C.J. Fan, Monitoring corn and soybean crop development with hand-held radiometer spectral data, Remote Sens. Environ 8 (3) (1979) 237–248, https://doi.org/10.1016/0034-4257(79)90004-X.
[51] A. Gitelson, N. Merzlyak, Quantitative experiments estimation of chlorophyll-u using reflectance with autumn chestnut and maple leaves and spectra, J. Photochem. Photobiol. B 22 (1994) 247–252, https://doi.org/10.1016/1011-1344(93)06963-4.
[52] J. Qi, A. Chehbouni, A.R. Huete, Y.H. Kerr, S. Sorooshian, A modified soil adjusted vegetation index, Remote Sens. Environ. 48 (2) (1994) 119–126, https://doi.org/10.1016/0034-4257(94)90134-1.
[53] B.-C. Gao, NDWI—A normalized difference water index for remote sensing of vegetation liquid water from space, Remote Sens. Env. 58 (3) (1996) 257–266, https://doi.org/10.1016/S0034-4257(96)00067-3.
[54] G. Rondeaux, M. Steven, F. Baret, Optimization of soil-adjusted vegetation indices, Remote Sens. Environ. 55 (2) (1996) 95–107, https://doi.org/10.1016/0034-4257(95)00186-7.
[55] A. Tassi, M. Vizzari, Object-oriented LULC classification in Google Earth Engine combining SNIC, GLCM, and machine learning algorithms, Remote Sens. (Basel) 12 (22) (2020) 3776.
[56] I. Guyon, J. Weston, S. Barnhill, V. Vapnik, Gene selection for cancer classification using support vector machines, Mach. Learn. 46 (2002) 389–422, https://doi.org/10.1023/A:1012487302797.
[57] M. Kuhn, Building predictive models in R using the caret package, J. Stat. Softw. 28 (5) (2008) 1–26, https://doi.org/10.18637/jss.v028.i05.
[58] L. Breiman, Random forests, Mach. Learn. 45 (2001) 5–32. https://link.springer.com/content/pdf/10.1023/a:1010933404324.pdf.
[59] M. Story, R. Congalton, Accuracy Assessment: a user's perspective, ISPRS J. Photogramm. Remote Sens. 52 (1986) 397–399.
[60] H. Xu, Modification of normalised difference Water Index (NDWI) to enhance open water features in remotely sensed imagery, IJRS 27 (14) (2006) 3025–3033, https://doi.org/10.1080/01431160600589179.
[61] L. Nhamo, J. Magidi, C. Dickens, Determining wetland spatial extent and seasonal variation of inundated area using multispectral remote sensing, Water SA 43 (4) (2017) 543, https://doi.org/10.4314/wsa.v43i4.02.
[62] Environmental Systems Research Institute (ESRI), ArcGIS Pro 3.0 software. ESRI, California, United States of America, 2020.
[63] J-P. Puyravaud, Standardizing the calculation of the annual rate of deforestation, For. Ecol. Manage. 177 (1–3) (2003) 593–596, https://doi.org/10.1016/S0378-1127(02)00335-3.
[64] D.A. Keith, C. Orscheg, C.C. Simpson, P.J. Clarke, L. Hughes, S.J. Kennelly, R.E. Major, T.R. Soderquist, A.L. Wilson, M. Bedward, A new approach and case study for estimating extent and rates of habitat loss for ecological communities, Biol. Cons. 142 (2009) 1469–1479, https://doi.org/10.1016/j.biocon.2009.02.015.
[65] C.J. Armando, Z. Yu, A.F. Mavume, V. Ongoma, A.M. Nyongesa, Formation and track of tropical cyclones Eline (2000) and Bonita (1996), Meteorol. Atmos. Phys. 133 (6) (2021) 1691–1706, https://doi.org/10.1007/s00703-021-00835-9.
[66] M. Ndlovu, M. Demlie, Hydrogeological characterization of the Kosi Bay Lakes system, north-eastern South Africa, Environ. Earth Sci. 75 (19) (2016) 1334, https://doi.org/10.1007/s12665-016-6164-6.
[67] J.R. Anderson, A Land Use and Land Cover Classification System For Use With Remote Sensor Data, 964, US Government Printing Office, 1976.
[68] X. Zhang, L. Liu, T. Zhao, J. Wang, W. Liu, X. Chen, Global annual wetland dataset at 30 m with a fine classification system from 2000 to 2022, Sci. Data 11 (1) (2024) 310, https://doi.org/10.1038/s41597-024-03143-0.
[69] A. Li, K. Song, S. Chen, Y. Mu, Z. Xu, Q. Zeng, Mapping African wetlands for 2020 using multiple spectral, geo-ecological features and Google Earth Engine, ISPRS J. Photogramm. Remote Sens. 193 (2022) 252–268, https://doi.org/10.1016/j.isprsjprs.2022.09.009.